HiSST: 3rd International Conference on
High-Speed Vehicle Science Technology
14 -19 April 2024, Busan, Korea

Cavity-based Combustion Characteristics of a Mach 10 Scramjet

Hongbo LU[1], Hengyi WU[2], Jian LIN[3], Ruiting WANG[4], Feng JI[5], Xing CHEN[6]

Abstract: To promote the efficiency of highly supersonic combustion of high Mach number scramjets, this study highlighted the crucial role of the flame stabilization and heat release enhanced by the cavity-aft shock pattern. A three-dimensional scramjet model was designed, which included a combustor with a constant width and a symmetrical-configured-cavity. The combustion characteristics of the hydrogen jet upstream of the cavity in the highly supersonic crossflow were investigated using OH* chemiluminescence combined with wall pressure measurements at the nominal simulated condition of Ma10 in free-piston driven high enthalpy shock tunnel. The evolution of hydrogen combustion, flame-stabilization structure, and heat release characteristics are presented. From the dynamic characteristics of OH* emission, it is found that the so-called "shock tube flow-combustion" mechanism is formed at the immediate moment when the freestream flow entering the scramjet, due to the employment of the fuel injection before the arrival of the mainstream crossflow. This mechanism results in an absolutely different ignition mechanism from the one during the process of fuel injection after the crossflow absolutely establishes. In spite of this phenomenon, the flame still stabilizes in the bodyside jet wake and the whole flowpath height around the cavity aft under the coupling effect of the self-ignition from the high total temperature and cavity-aft X-type shock pattern when the interaction of fuel jet with the highly supersonic crossflow tends to a quasi-steady regime. The wall pressure rise characteristics induced by heat release reveals that the combustion inside the engine is in a pure supersonic combustion mode, and a maximum heat release rate occurs around the cavity, indicating the combustion is enhanced by the cavity-aft X-type shock pattern. These results of cavity-aft-shock enhanced combustion in a Ma10 supersonic combustor can be aid in design of high-performance combustion for high Mach number scramjets.

Keywords: Cavity-aft-shock enhanced combustion, Scramjet, Chemiluminescence diagnostics, High enthalpy shock tunnel

Nomenclature

C – mass fraction
Ma – Mach number
P – Pressure
T - Temperature
ER – Equivalence ratio
U – Velocity
ρ – Density
Subscripts
∞ – freestream conditions
t – total conditions

1. Introduction

As one of the key technologies for air-breathing hypersonic aircraft, the scramjet has drawn an ever increasing attention. Since the verification of supersonic combustion completed by Ferri[1], a large

[1] *China Academy of Aerospace Aerodynamics, Beijing 100074, China, E-mail: finlhb_0605@163.com*
[2] *China Academy of Aerospace Aerodynamics, Beijing 100074, China, E-mail: 1966912073@qq.com*
[3] *China Academy of Aerospace Aerodynamics, Beijing 100074, China, E-mail: naoh52@sohu.com, corresponding author*
[4] *China Academy of Aerospace Aerodynamics, Beijing 100074, China, E-mail: 623324632@qq.com*
[5] *China Academy of Aerospace Aerodynamics, Beijing 100074, China, E-mail: jifeng_caaa@163.com*
[6] *China Academy of Aerospace Aerodynamics, Beijing 100074, China, E-mail: chenxing0234@sina.com*

amount of work has been conducted worldwide to advance the mature of scramjet technologies. Flight tests demonstrated that it is feasible to achieve net thrust for moderate Mach number scramjets, whereas it is still an open issue for scramjets operating at a flight Mach number over 8. In a high Mach number scramjet combustor, the poor efficiency in fuel mixing and combustion released heat become dramatically salient due to the harsh conditions of ultra-high speed(~3km/s), low air pressure(~0.3atm), and extremely short residence time(~0.5ms)[2-3]. To facilitate this issue being resolved, many technical and theoretical methods have been proposed by the University of Queensland, such as inlet injection[4-11], boundary layer injection and combustion[12-13], non-uniform customized injection[14], and porous media and oxygen-enriched injection[15-17]. These techniques were employed in an airframe-integrated scramjet with a rectangular-to-elliptical shape transition (REST) operating at a wide range of Mach number between 6 and 12, and notably improve the REST engine performance according to series of semi/full free jet tests in T4 shock tunnel. Another systematic trimmed theory of the inlet compression ratio and the combustor flowpath contour was presented by Takahashi[18-19] to reduce endothermic dissociation and achieve a tuned heat release, which was confirmed through free jet tests of the Ma12-0X series engine in the HIEST shock tunnel. A nonuniform compression was explored by Bricalli[20], Vanyai [21,22] to take advantage of thermal compression effects, which successfully enabled the flame to be propagated into the low-compression region through three-dimensional flow–combustion interactions. The performance of a strut-aided scramjet was numerically studied by Yao[23-25] for a wide range of flight Mach number between 7 and 10. From Yao's work, fuel mixing efficiency at high Mach numbers was significantly enhanced. A shock-induced combustion ramjet (shcramjet) was proposed by Menees[26] and Dudebout[27] to realize a detonation in wave combustor, and was numerically proved to be obtain high specific impulse for a flight Mach number over 10[28-29] . Hypermixer injectors designed by Takahashi[19] were applied to a Ma12-02 scramjet engine to obtain a high efficient combustion through generating streamwise vortices to enhance fuel/air mixing in high supersonic flows, resulting in a remarkable improvement of flame stability and ignition capability. To understand physical mechanisms from ignition to flame holding induced hypermixer, numerical studies by Kodera[30], Zhang[31], Hiejima[32] and Liu[33] were performed and diamond-shaped shock patterns from hypermixer are highlighted in the importance of shock-aided flame stabilization, which is also the focus of the current paper.

In our paper, the cavity-aft shock patterns were employed to improve a scramjet performance at high Mach number conditions. A three-dimensional scramjet model was designed to explore cavity-aft shock-enhanced combustion, where a rectangular combustor with a symmetrically both-side-configured cavity. Several free-jet tests were conducted to obtain combustion characteristics at the nominal Mach number of 10 in free-piston driven high enthalpy shock tunnel. The OH* chemiluminescence diagnostics were used to characterize the time-evolving and quasi-steady flame features of the hydrogen jet injected upstream of the cavity in a supersonic crossflow of the scramjet combustor, together with the corresponding heat release regime.

2. Experimental setup

2.1. Experimental flow conditions

The experiments presented here were conducted in free-piston driven high enthalpy shock tunnel of China Academy of Aerospace Aerodynamics (CAAA). The free-piston driven shock tunnel is a Stalker tube, whose structure and operation principle can be referred the literature[34]. A contoured axisymmetric nozzle with an exit diameter of φ1.2m was adopted to generate the hypervelocity flow at the nominal Mach number of 10. Due to the notorious difficulty to characterize and control on a shot-to-shot basis, freestream flow parameters such total pressure and the incident shock velocity were measured each shot. The total pressure of the test gas was directly measured by Kulite sensors with a full scale (FS) of 60MPa and an accuracy of ±1% FS, which locates at the end of the driven shock tube. The incident shock velocity was measured as the times of flight between shock counters mounted along the driven tube. The experimental conditions listed in Table 1 was detailed from the average values of total pressure and total temperature for all shots with the aid of numerical simulation using the two-temperature air-dissociation developed by Park[35]. A vibrational nonequilibrium as well as some oxygen atom exist in the freestream, but will not affect the bulk flame characteristics[36,37].

Table 1. Experimental conditions of the nominal Mach number of 10

Ma_∞	P_∞ (Pa)	ρ (kg/m^3)	T_∞ (K)	$T_{vib,\infty}$ (K)	U_∞ (m/s)	$C_{N2,\infty}$ (%)	$C_{O2,\infty}$ (%)	$C_{NO,\infty}$ (%)	$C_{O,\infty}$ (%)	$C_{N,\infty}$ (%)
9.50	375	4.60E-3	283	1590	3107	73.93	19.95	5.96	0.16	0.00

2.2. A nose-to-tail three dimensional scramjet model

A nose-to-tail three-dimensional scramjet model was employed, which consists of a three-dimensional inlet, a rectangular isolator and combustor, and a nozzle, as shown in Fig. 1. The minimum cross-sectional height of the scramjet flowpath is 20mm (H=20mm). The width is maintained at a constant value of 90mm. The three-dimensional curved surface of the inlet was designed using streamline tracing. The compression surface gradually widens from the leading edge and then gradually narrows to the capture width of 90mm. A rearward inclination in the sidewall of the scramjet is designed to automatically exclude the boundary layer, reducing the boundary layer separation from the cowl-lip shock. An ideal capture area of 0.018m^2 is realized by the inlet. The isolator is a micro-expansion, constant-width channel with an entrance height of 20mm and a divergence angle of 0.76°. The combustion chamber is a rectangular channel with dual side cavities, micro-expansion, and constant width. The upstream expansion angle of the cavity is 0.76°, and the downstream expansion angle is 1.83°. The depth of the cavity is 5mm, with a length-to-depth ratio of 5 and a trailing edge angle of 45°. Two quartz windows (GS1) with a length of 110mm are arranged around the cavity and downstream in the combustion chamber to visualize OH* chemiluminescence features. The nozzle is a variable cross-section tube, with a rectangular entrance of 36mm×90mm and a circular exit with a radius of 140mm. On the scramjet bodyside wall, 38 pressure sensors are arranged, labeled as P_1 to P_{38}, covering the inlet (P_1 to P_{15}), isolator (P_{16} to P_{19}), combustor (P_{20} to P_{32}), and nozzle (P_{33} to P_{38}) sections. Two types of pressure transducers were used, leading to a difference in the response time. Therefore, the effective sampling time was deemed as the quasi-plateau period that both types of pressure transducers reached.

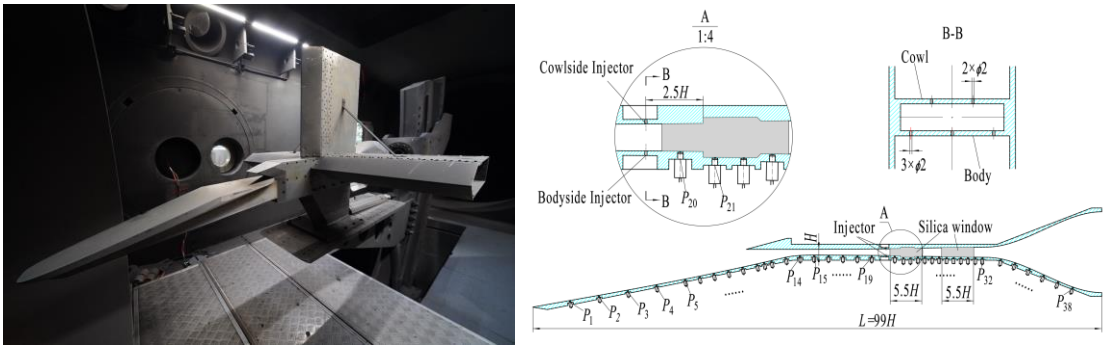

Fig 1. The scramjet test article, the left is an assembly structure in free-piston driven shock tunnel, the right is the layout of injectors

The hydrogen injector was located at 2.5 times the height of the throat (2.5H in the magnified view of Fig. 1) upstream of the throat height. Gaseous hydrogen was perpendicularly injected into the highly supersonic mainstream flow through 5 portholes with a diameter of φ2mm. Specifically, 3 holes are evenly distributed on the bodyside wall, and 2 holes are evenly distributed on the cowlside wall. The pressure of the injected hydrogen was measured to calculate the fuel mass flow rate assuming the sonic jet conditions. Due to the short available time duration of a high enthalpy shock tunnel, fuel injection was controlled by a fast-acting solenoid valve which was triggered from the pressure jump signal on the driver tube wall. The fuel jet is established in the scramjet before the arrival of the freestream hypervelocity flow, and the pressure at the plenum of bodyside and cowlside injectors remains approximately constant during the establishment of the air freestream flow. Fig. 2 presents the typical time history of the hydrogen-injection stagnation pressure (P_{inj}), air-freestream stagnation pressure (P_t) and the isolator wall pressure(P_{19}).

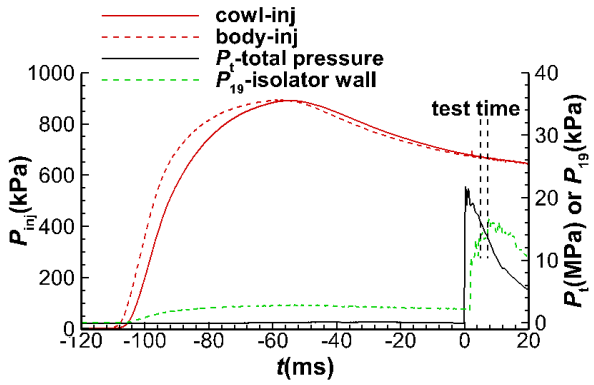

Fig 2. The typical time traces of the hydrogen-injection stagnation pressure (P_{inj}), air-freestream stagnation pressure (P_t) and the isolator wall pressure(P_{19})

2.3. OH* chemiluminescence imaging approach

A large number of excited free radicals are generated in the chemical reaction process such as OH*, CH*[38-39]. Their emission intensity is related to the amount of the excited species, which can be correlated to the ignition and flame characteristics. In this study, OH* (excited hydroxyl) chemiluminescence was employed to investigate the cavity-based combustion characteristics of a Mach 10 scramjet. OH* emission signal was in the ultraviolet spectrum from naturally occurring chemically excited hydroxyl radicals as they decay from the $A^2\Sigma^+$ excited electronic state to the $X^2\Pi$ ground state through spontaneous radiative emission. The UVi Series 1850 image intensifier was equipped to the imaging system of a Photron FASTCAM SA-Z camera, an UV lens aperture, and a band-pass filter. The filter was centered at 307nm with a half full width of 10nm (307nm±10nm). Due to the limit of the short test time, the Photron FASTCAM SA-Z camera, together with data acquisition system was synchronized using a DG645 signal generator. The DG645 signal generator is triggered when the voltage of the total pressure sensor reached the value of 1.2V, which serves as the zero point of time axis during the experimental process. The exposure time of the UVi image intensifier is set to 25μs, and an exposure time of the SA camera was dependent on the recording frame rate while keeping a minimum exposure time of 50μs. A line-of-sight-integrated image of the overall location of the burning regions was obtained by an 8-bit depth for all shots.

In this work, the OH* chemiluminescence was used as an approximate indicator of the global heat release distribution in the flow field. No calibration to relate heat release rate to emission intensity has been attempted and the reported results are used to draw conclusions based on a relative scale. Therefore, in order to allow for a direct comparison between different cases, the imaging configuration (such as magnification, field of view, etc.) and camera settings (such as gain on the intensifier, camera lens aperture, etc.) were maintained unaltered between all cases considered in the study.

3. Results and discussion

Four cases were obtained under the experimental conditions shown in Table 1, as shown in Table 2, one of which was the tare case without fuel injection (ER=0) and the others with hydrogen injection. The total pressure is the time-averaged value o during the available test time. The total temperature is obtained according to the total pressure and the incident shock velocity at the driven tube end.

Table 2. Experimental Overview of the selected freejet tests

Shot	Case	P_t(MPa)	T_t(K)	$P_{inj\text{-}cowl}$(kPa)	$P_{inj\text{-}body}$	*ER*
2313	A	18.92	4084	0		0
2315	B	19.12	4091	669.4	665.6	0.87
2316	C	19.20	4168	623.8	621.2	0.81
2318	D	19.42	4176	628.8	631.3	0.81

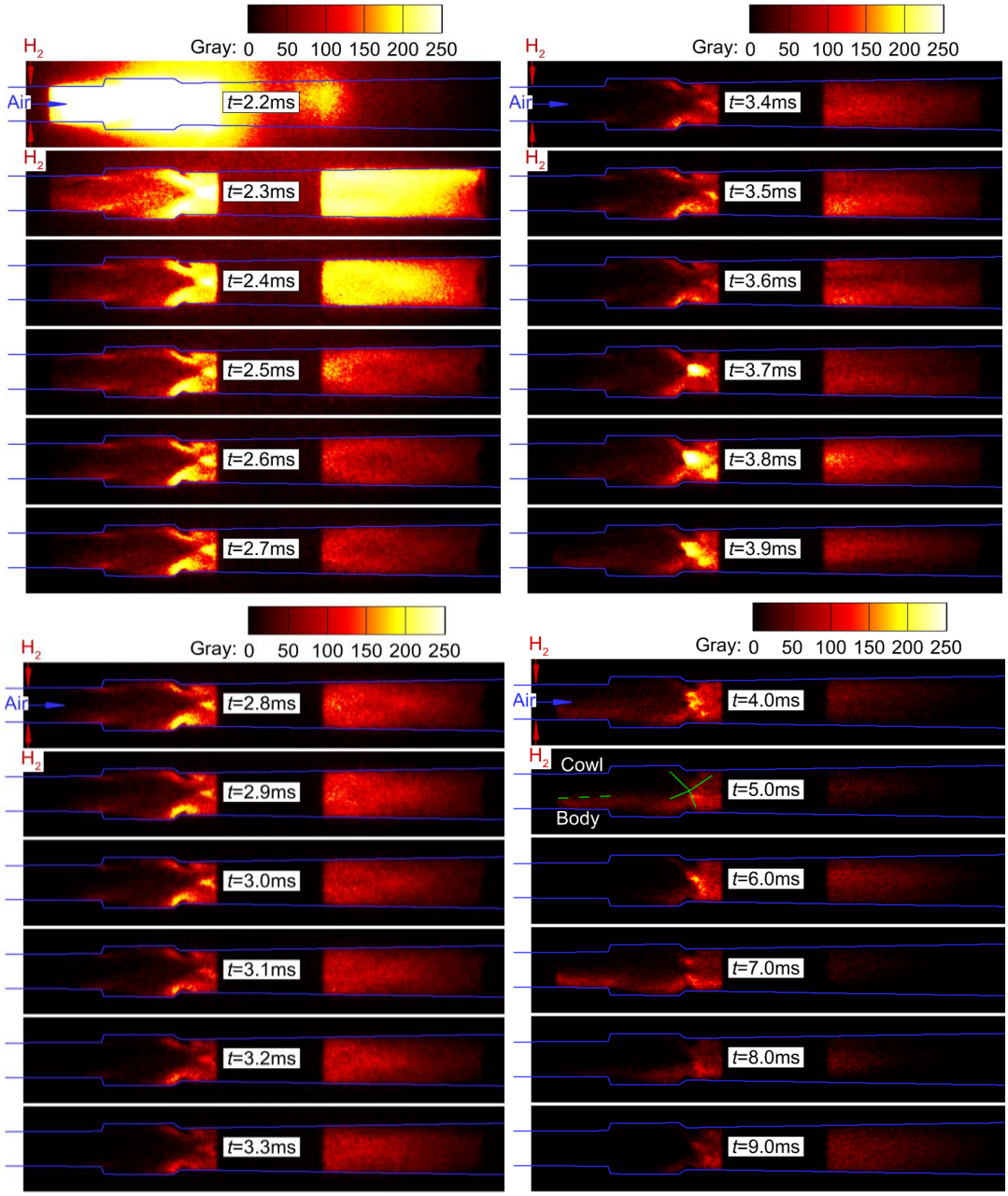

Fig 3. OH* luminosity features across t=2.2ms~9ms recorded by a frequency of 10kHz for case B

3.1. Combustion evolving characteristics

Fig. 3 shows the time-evolving characteristics of OH* emission images inside the scramjet combustor for Case B. The grayscale value of the image represents OH* emission intensity, indicating the burning regions and the heat release extent. It can be seen that during the establishment of the mainstream airflow (t=2.2ms~3.8ms in Fig. 3), the OH* radical exhibits a symmetrical flame patterns, and the luminosity gradually weakens with the gradual establishment of the mainstream airflow, indicating that the flame structure during this period is not affected by the asymmetric influence of the airflow and hydrogen jet, and presents a symmetrical combustion. After the coupling flow field of the mainstream airflow and hydrogen jet becomes stable (t=4ms~7ms in Fig. 3), the OH* radical exhibits a significant asymmetrical distribution, mainly concentrated in the near-wall area of the compression surface upstream of the cavity and the full flow field near the trailing edge of the cavity, and the OH* concentration near the trailing edge of the cavity is larger, indicating that the flame is stable in the near-wall jet wake and the full height combustor near the trailing edge of the cavity after the flow field tends to a quasi-steady regime. During the whole process, the flame around the cavity aft part remains

a constant existence and does not extinguish, indicating that the X-type shock pattterns from the cavity trailing edge plays the role of a flame stabilizer.

Due to the employment of the fuel injecting before the arrival of the mainstream airflow, the scramjet is filled with a large amount of hydrogen, which is confirmed by the pressure characteristics at measurement point P_{17} in the isolation section as shown in Fig.4 (at t<2ms, the pressure difference inside the isolation section with and without hydrogen injection is about 1.8kPa~2kPa). Consequently, at the moment when the mainstream hypervelocity airflow reaches the inside of the engine, a phenomenon called "shock tube flow-combustion" is formed, as shown in Fig. 5, where the mainstream airflow acts as the driving gas, and the hydrogen gas acts as the driven gas. The region on both sides of the contact is divided into high-temperature hydrogen gas heated by the incident shock wave and high-total-temperature airflow. Self-ignition and combustion occur in the region where the hydrogen gas and the airflow mix near the contact in this approximate shock tube flow-combustion process. In this ignition and combustion starting up process, the spatial distribution difference between hydrogen gas and airflow is relatively small, and the flame structure is relatively uniform and symmetrical (t=2.2ms~2.4ms in Fig. 3).

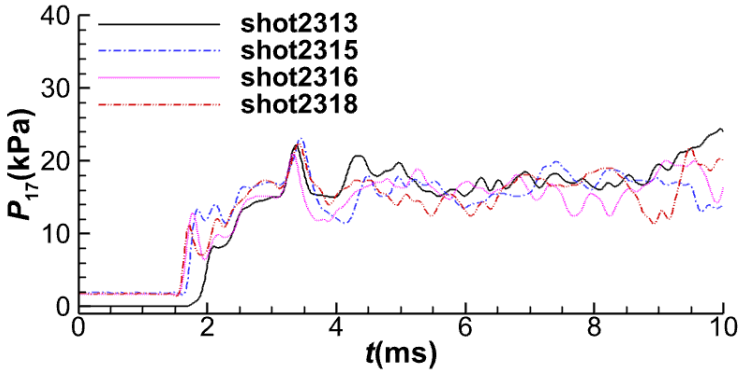

Fig 4. Time traces of wall pressure at P_{17} inside the isolator upstream of the injector for different shots

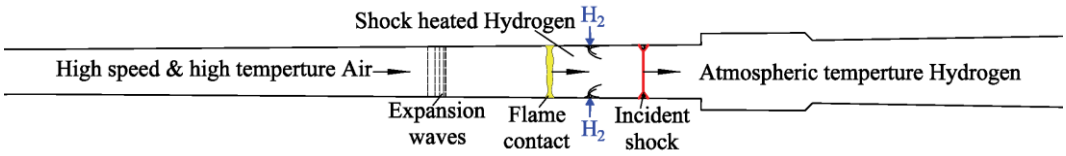

Fig 5. Shock tube flow-combustion formed at the immediate moment of the hypervelocity airflow arriving the inside of the engine

As the mainstream air flows downstream, this "shock tube flow-combustion" gradually disappears, and the relatively weak combustion in the near-wall region between the injection location and the cavity becomes difficult to sustain and gradually extinguishes. However, the combustion around the cavity aft part continues to be maintained (t=2.4ms~3.3ms in Fig. 4). With the further establishment of the mainstream airflow, the jet wake in the near-wall region between the injection location and the cavity ignites again (t=3.4ms~3.9ms in Fig. 4). When the interaction between the mainstream airflow and the wall-injected hydrogen jet completely establishes, the flame stabilizes in the region of the hydrogen jet wake on the bodyside side and the whole flowpath around the cavity aft part for the available test time (t=4ms~7ms in Fig. 4). When the available test time ends, the burning of the hydrogen jet wake is broken, while the flame induced from cavity-aft X-type shock pattern is still kept. These time-evolving characteristics demonstrate that the combustion occupied in the whole height of the combustor is achieved by cavity-aft X-type shock pattern, enhancing the combustion.

3.2. Flame stabilized structure

Referring to the CH* emission image processing used by Yuan[38], statistical analysis was performed on the OH* images during the effective test time, and the statistical averages and standard deviations of the flame characteristics were obtained as shown in Fig. 6. Through the statistical analysis of the OH* radiation information at each spatial point during the approximate steady flow period, it

was found that the flame remained stable in the region of the bodyside jet wake and the X-type shock structure at the trailing edge of the cavity, and the combustion induced by the X-type shock wave was more intense. The work of Gamba [56] indicated that at high total temperature conditions (3000K), the ignition and flame stabilization structure mainly depended on the momentum ratio of the fuel jet to the mainstream crossflow. When this ratio was low, the flame stabilized in the near-wall region of the jet wake far downstream from the injection location. When this ratio was large, the flame stabilized in the jet-induced separation region upstream of the injection location and the downstream jet wake region. Considering the experimental conditions of this study, it can be concluded that the aforementioned flame stabilization structures are formed by the combined effects of high total temperature ignition and the X-type shock pattern at the trailing edge of the cavity. The difference in the near-wall flame structure between the bodyside and the cowlside is caused by the significantly different boundary layer thickness on both sides, resulting in significantly different momentum ratios between the fuel jet and the crossflow. The development distance of the boundary layer on the bodyside wall is 2.5 times of the cowlside wall, resulting in a relatively smaller momentum of the crossflow on the bodyside, while the hydrogen jet momentum on both sides is approximately the same (the measured injection stagnation pressure is approximately consistent). Therefore, the momentum ratio on the bodyside is large enough to induce the occurrence of burning at the injection location as well as the jet wake region, while the momentum ratio on the cowlside is so low that a lifted-off flame occurring far downstream and being enhanced by the X-type shock patterns at the trailing edge of the cavity.

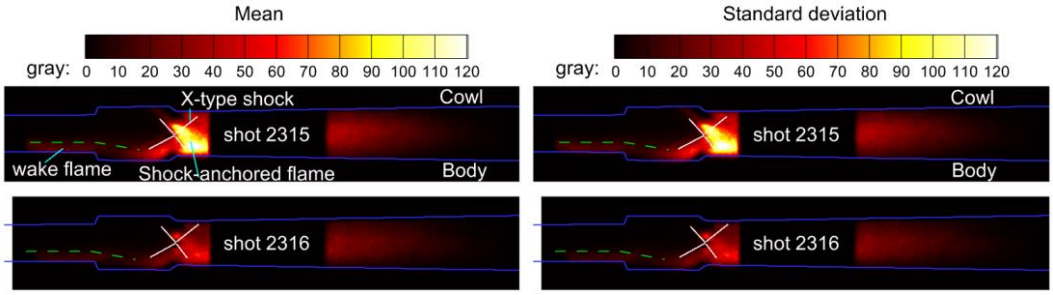

Fig 6. Statistical characteristics of flame structure during the effective test time

3.3. Heat release analysis from wall pressure distribution Characteristics

The time-averaged pressure and standard deviation were collected and the pressure distributions on the bodyside wall were gained, shown in Fig. 7. The vertical axis represents the absolute pressure, which was corrected for the differences in total pressure between each shot. The wall pressure of each shot is normalized by the corresponding total pressure and then multiplied by the average total pressure of all shots. The horizontal axis represents the streamwise distance dimensioned by the scramjet length. It is worth noting that the pressure inside the cavity and approaching the leading edge of the cavity is consistently lower but there are significant differences between the cold and hot shots, making it difficult to determine whether these differences results from the flow characteristics or sensor anomalies. Therefore, the data was retained.

From Fig.7, it is observed that the wall pressure upstream of the hydrogen injection ($x/L<0.594$) is approximately identical for cold and hot shots, while there is a remarkable pressure jump induced by combustion from the hydrogen injection location to the nozzle exit. The features in the wall pressure distribution reveals that the flow upstream the hydrogen injection cannot be disturbed by the combustion behaviors downstream, and the combustion inside the engine is in a pure supersonic combustion mode. The maximum pressure rise occurs in the combustion zone induced by the X-type shock pattern, which is consistent with the OH* radical emission intensity in the flame structure in Fig. 6, further indicating that the cavity enhances combustion through the X-type shock under high Mach number conditions.

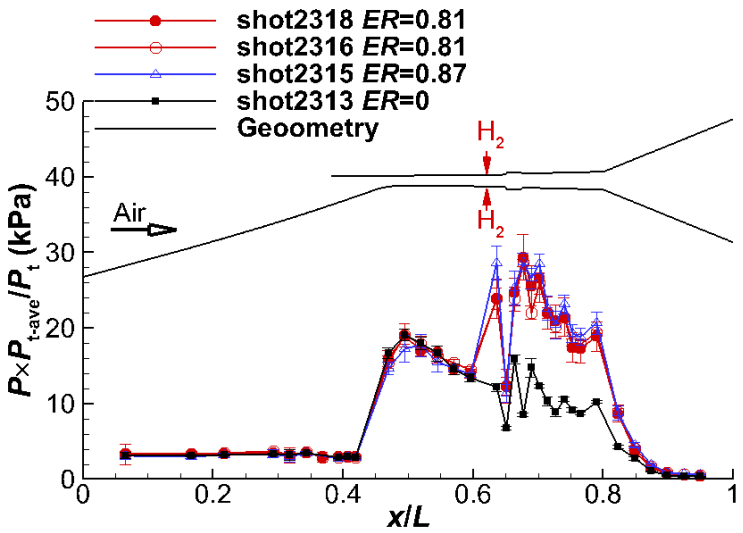

Fig 7. Wall pressure distributions of the scramjet bodyside for different shots

4. Conclusions

In this study, we investigated the combustion characteristics of a hydrogen jet upstream of a cavity combustor under the hypervelocity conditions of Ma9.5, static pressure of 375Pa, and velocity of 3.1km/s using OH* spontaneous emission spectroscopy and wall pressure measurement of free-piston driven high enthalpy shock tunnel. The evolution of hydrogen combustion, flame-stabilized structure, and heat release-induced pressure rise were presented. Due to the employment of the fuel injection before the arrival of the mainstream crossflow, the scramjet is filled with a large amount of hydrogen, forming the so-called "shock tube flow-combustion" mechanism at the immediate moment when the freestream flow entering the scramjet. The ignition and combustion characteristics presents a symmetrical flame pattern with a gradual reduction of OH* luminosity at the initial period of the freestream flow startup, leading to an absolutely different ignition mechanism from the one during the process of fuel injection after the crossflow absolutely establishes. However, when the interaction of fuel jet with the highly supersonic crossflow tends to a quasi-steady regime, the flame stabilizes in the bodyside jet wake and the whole flowpath height around the cavity aft under the coupling effect of the self-ignition from the high total temperature and cavity-aft X-type shock pattern. The wall pressure rise characteristics induced by heat release reveals that the combustion inside the engine is in a pure supersonic combustion mode, and a maximum heat release rate occurs around the cavity, indicating the combustion is enhanced by the cavity-aft X-type shock pattern. These results of cavity-aft-shock enhanced combustion in a Ma10 supersonic combustor can be aid in design of high-performance combustion for high Mach number scramjets.

References

1. Ferri A: Review of scramjet propulsion technology[J]. Journal of Aircraft, 1968, 5(1): 3-10
2. Urzay J: Supersonic combustion in air-breathing propulsion systems for hypersonic flight. Annual Review of Fluid Mechanics, 2018, 50:593-627
3. Liu Q, Baccarella D, Lee T: Review of Combustion Stabilization for Hypersonic Airbreathing Propulsion. Progress in Aerospace Sciences, 2020, 119:100636
4. Suraweera M, Smart M. Shock-Tunnel Experiments with a Mach 12 Rectangular-to-Elliptical Shape-Transition Scramjet at Off-design Conditions. Journal of Propulsion and Power, 2009, vol. 25, pp. 555–564.
5. Doherty, L. (2013). Experimental Investigation of an Airframe Integrated 3-D Scramjet at a Mach 10 Flight Condition. Ph.D. thesis, School of Mechanical and Mining Engineering, The University of Queensland.

6. Doherty, L.; Smart, M. and Mee, D. (2012a). "Design of an Airframe Integrated 3-D Scramjet and Experimental Results at a Mach 10 Flight Condition". In AIAA (Ed.), 18th AIAA/3AF International Space Planes and Hypersonic Systems and Technologies Conference. AIAA 2012-5910.
7. Wise D. Experimental Investigation of a Three Dimensional Scramjet Engine at Hypervelocity Conditions. Ph.D. thesis, School of Mechanical and Mining Engineering, The University of Queensland, 2014.
8. Turner, J. (2010). An Experimental Investigation of Inlet Fuel Injection in a Three-Dimensional Scramjet Engine. Ph.D. thesis, Division of Mechanical Engineering
9. Turner, J. and Smart, M. (2010). "Application of Inlet Injection to a Three-Dimensional Scramjet at Mach 8". AIAA Journal, vol. 48, no. 48, pp. 829–838
10. Barth JE, Wheatley V, Smart MK. Effects of hydrogen fuel injection in a Mach 12 scramjet inlet. AIAA Journal, 2015, 53(10): 2907-2919
11. Landsberg WO, Wheatley V, Smart MK, et al. Enhanced supersonic combustion targeting combustor length reduction in a Mach 12 scramjet. AIAA Journal, 2018, 56(10): 3802-3807
12. Kirchhartz R, Mee D, Stalker R. Supersonic skin-friction drag with tangential wall slot fuel injection and combustion[J]. AIAA Journal, 2012, 50(2): 313-324.
13. Barth J, Wheatley V, Smart M. Hypersonic turbulent boundary-layer fuel injection and combustion: skin-friction reduction mechanisms[J]. AIAA Journal, 2013, 51(9): 2147-2157.
14. Barth J, Wise D, Wheatley V, et al. Tailored fuel injection for performance enhancement in a Mach 12 scramjet engine[J]. Journal of Propulsion and Power, 2018, 35(1): 1-15.
15. Razzaqi S, Smart M. Hypervelocity experiments on oxygen enrichment in a hydrogen-fueled scramjet[J]. AIAA Journal, 2011, 49(7): 1488-1497.
16. Petty D, Wheatley V, Smart M, et al. Effects of oxygen enrichment on scramjet performance[J]. AIAA Journal, 2013, 51(1): 226-235.
17. Capra B, Boyce R, Kuhn M, et al. Combustion enhancement in a scramjet engine using oxygen enrichment and porous fuel injection[J]. Journal of Fluid Mechanics, 2015, 767: 173-198.
18. Takahashi M, Sunami T, Hideyuki T, et al. Performance Characteristics of a Scramjet Engine at Mach 10 to 15 Flight Condition[C]. AIAA/CIRA 13th International Space Planes and Hypersonics Systems and Technologies Conference, AIAA 2005-3350, 2005.
19. Takahashi M, Komuro T, Sato K, et al. Performance Characteristics of Scramjet Engine with Different Combustor Shapes at Hypervelocity Condition over Mach 10 Flight[C]. 43rd AIAA/ASME/SAE/ASEE Joint Propulsion Conference & Exhibit, AIAA 2007-5395, 2007.
20. Bricalli, M. G., Brown, L. M., and Boyce, R. R., "Supersonic Combustion Processes in a Premixed Three-Dimensional Nonuniform-Compression Scramjet Engine," AIAA Journal, Vol. 52, No. 8, 2014,pp. 1670–1685. https://doi.org/10.2514/1.J052640
21. Vanyai T. Experimental investigation of 3D thermal compression scramjet using advanced optical techniques[D]. St. Lucia, QLD, Australia: School of Mechanical and Mining Engineering, The University of Queensland, 2018.
22. Vanyai T, Brieschenk S, Bricalli M, et al. Thermal compression effects within a fundamental, hydrogen-fuelled scramjet[J]. Aerospace Science and Technology, 2021, 110: 106499.
23. Yao, W., Liu, H., Xue, L., and Xiao, Y., "Performance Analysis of a Strut-Aided Hypersonic Scramjet by Full-Scale IDDES Modeling," Aerospace Science and Technology, Vol. 117, Oct. 2021, pp. 1–14. https://doi.org/10.1016/j.ast.2021.106941
24. Yao,W., Liu, H., Li, L., and Yue, L., "NonequilibriumEffect Modeling in High-Ma Scramjet Based on Dynamic Zone Model," AIAA Paper 2021-3543, 2021. https://doi.org/10.2514/6.2021-3543
25. Yao W, Liu H, Zhang Z, et al. Effects of Thermal/Chemical Nonequilibrium on a High-Mach Ethylene-Fueled Scramjet. JOURNAL OF PROPULSION AND POWER, Vol. 39, No. 4, July–August 2023, 562-579.

26. Menees, G. P., Adelman, H. G., Cambier, J.-L., and Bowles, J. V., "Wave Combustors for Trans-Atmospheric Vehicles," Journal of Propulsion and Power, Vol. 8, No. 3, 1992, pp. 709–713. https://doi.org/10.2514/3.23536

27. Dudebout, R., Sislian, J. P., and Oppitz, R., "Numerical Simulation of Hypersonic Shock-Induced Combustion Ramjets," Journal of Propulsion and Power, Vol. 14, No. 6, 1998, pp. 869–879. https://doi.org/10.2514/2.5368

28. Alexander, D. C., and Sislian, J. P., "Computational Study of the Propulsive Characteristics of a Shcramjet Engine," Journal of Propulsion and Power, Vol. 24, No. 1, 2008, pp. 34–44. https://doi.org/10.2514/1.29951

29. Chan, J., Sislian, J. P., and Alexander, D., "Numerically Simulated Comparative Performance of a Scramjet and Shcramjet at Mach 11," Journal of Propulsion and Power, Vol. 26, No. 5, 2010, pp. 1125–1134. https://doi.org/10.2514/1.48144

30. Kodera, M., Yang, V., Takahashi, M., and Itoh, K., "Ignition Transient Phenomena in a Scramjet Engine at Mach 12 Flight Condition," AIAA Paper 2007-5407, 2007. https://doi.org/10.2514/6.2007-5407

31. Zhang, S., Li, J., Qin, F., Huang, Z., and Xue, R., "Numerical Investigation of Combustion Field of Hypervelocity Scramjet Engine," Acta Astronautica, Vol. 129, Dec. 2016, pp. 357–366. https://doi.org/10.1016/j.actaastro.2016.09.028

32. Hiejima T, Oda T. Shockwave effects on supersonic combustion using hypermixer struts. Physics of Fluids, 2020, 32(1): 016104

33. Liu, Y., He, X., Feng, L., Xue, R., Zhang, Y., Xu, C., and Du, J.,"Numerical Simulation of the Interaction between Shock Train andCombustion in Three-Dimensional M12-02 Scramjet Model," International Journal of Hydrogen Energy, Vol. 47, No. 12, 2022, pp. 8026–8036. https://doi.org/10.1016/j.ijhydene.2021.12.126

34. Lu HB Chen X, Li Chen, et al. Preliminary commissioning of hydrogen supersonic combustion in FD-21 free piston driven shock tunnel. Proc. of the 32nd International Syposium on Shock Waves (ISSW32).

35. Park C. Review of chemical-kinetic problems of future NASA missions. I - Earth entries. Journal of Thermophysics and Heat Transfer, 1996, 7(3): 385-398

36. Yu Ao, Kun Wu, Hongbo Lu, et al. Combustion dynamics of high Mach number scramjet under different inflow thermal nonequilibrium conditions. Acta Astronautica, 2023, 208: 281–295

37. Stalker RJ, Pall A, Mee DJ, et al. Scramjets and shock tunnels-The Queensland experience[J]. Progress in Aerospace Sciences, 2005, 41: 471-513.

38. Yuan YM, Zhang TC, Yao W, et al. Characterization of flame stabilization modes in ethylene-fueled supersonic combustor using time-resolved CH* chemiluminescence[J]. Proceedings of the Combustion Institute, 2016, 000:1–7.

39. Gamba M, Mungal GM. Ignition, flame structure and near-wall burning in transverse hydrogen jets in supersonic crocssflow[J]. Journal of Fluid Mechanics, 2015, 780:226–273.